

AIAA'83

from R.S.

st: blunt

AIAA-83-1763

NOSETIP BLUNTNESS EFFECTS ON CONE FRUSTUM
BOUNDARY LAYER TRANSITION IN HYPERSONIC FLOW

K.F. STETSON, FLIGHT DYNAMICS LAB,
WRIGHT-PATTERSON AFB, OHIO

AIAA 16th Fluid and Plasma Dynamics Conference

July 12-14, 1983
Danvers, Massachusetts

For permission to copy or republish, contact the American Institute of Aeronautics and Astronautics

1633 Broadway New York, NY 10019

NOSETIP BLUNTNESSE EFFECTS ON CONE FRUSTUM
BOUNDARY LAYER TRANSITION IN HYPERSONIC FLOW

Kenneth F. Stetson*
Flight Dynamics Laboratory
Air Force Wright Aeronautical Laboratories
Wright-Patterson AFB, Ohio

Abstract

The effects of nosetip bluntness on cone frustum boundary layer transition were investigated by conducting hypersonic wind tunnel experiments. Frustum transition Reynolds numbers were found to have large variations within the entropy layer swallowing region. The results from this investigation indicated that several nosetip blunting effects were competing for the dominant role in the frustum transition process and it was speculated that the large variations in transition Reynolds number were associated with the shifting of dominant roles. Based upon these studies, dominant nosetip blunting effects are tentatively identified with three regions of the entropy layer. (1) When transition occurred at locations where the entropy layer was nearly swallowed ($X_n/X_{SW} \sim 1$), the nosetip apparently had a stabilizing effect upon the boundary layer since transition Reynolds numbers greater than those of a sharp cone were obtained. (2) Further forward in the entropy layer ($X_n/X_{SW} \sim 0.1$), it appeared that more than one effect was important. Some unidentified effect was dominant, producing transition Reynolds numbers less than those of a sharp cone. To a lesser degree, the favorable pressure gradient generated by the nosetip was significant. Some variations in the magnitude of Re_{XT} could be related to the strength of the favorable pressure gradient. (3) In the early portion of the entropy layer swallowing region ($X_n/X_{SW} < .03$) frustum transition was dominated by the nosetip flow and surface conditions. Low transition Reynolds numbers were obtained in spite of the existence of a favorable pressure gradient. There were several characteristics of transition in this region which were different from the other two regions. Data are presented to illustrate the transition features of each of the three regions.

*Aerospace Engineer, High Speed Aero Performance Branch, Aeromechanics Division
Associate Fellow AIAA

Helpful discussions and suggestions from the Boundary Layer Transition Study Group are gratefully acknowledged. The paper was reviewed by N. Scaggs, E. Brown-Edwards and D. Bowers. Their suggestions for improving the paper are much appreciated.

Nomenclature

h	Local heat transfer coefficient (recovery temperature of $0.9 T_0$ assumed) (Btu/ft ² - sec°R)
k	Roughness height (inches)
M	Mach number
p	Surface pressure (psia)
q	Heat transfer rate (used in nondimensional ratio, \dot{q}/\dot{q}_{ST})
R	Radius (inches)
Re	Reynolds number
Re_{XT}	Transition Reynolds number based upon conditions at the edge of the boundary layer and surface distance from the sharp tip or stagnation point to the location of transition
Re_θ	Reynolds number based upon conditions at the edge of the boundary layer and the laminar boundary layer momentum thickness
t	Time (sec)
T	Temperature (°R)
X	Surface distance (inches)
X_{SW}	Entropy layer swallowing distance (see Figure 3) (inches)
X_T	Surface distance from the sharp tip or stagnation point to the onset of transition (inches)
X_{TB}	Surface distance to onset of transition on blunt configurations (inches)
X_{TS}	Surface distance to onset of transition on sharp configurations (inches)
α	Angle of attack (degree)
θ	Laminar boundary layer momentum thickness (inches)
θ_c	Cone half angle (degrees)

Subscripts

B	Base or blunt
e	Edge of boundary layer
N	Nose
O	Reservoir
S	Sharp
ST	Model stagnation point
W	Wall
∞	Free stream

1.0 Introduction

The transition of a boundary layer from laminar to a turbulent state is a complex phenomena which is influenced by many contributing factors. A number of excellent review papers have discussed the magnitude of this problem and the current understanding of stability and transition phenomena (e.g., Morkovin^{1,2,3} and Reshotko⁴). The importance of knowing the body location where the boundary layer changes from laminar to turbulent is well documented with examples of large changes in heat transfer rates, skin friction drag, and changes in stability and control effectiveness. In spite of many stability and transition investigations over the past years, boundary layer transition prediction remains an area of considerable uncertainty to vehicle designers. In a recent survey paper, Pate⁵ commented on the current ability to predict the occurrence of boundary layer transition. He estimated that transition could be adequately predicted in less than 20 percent of the times attempted. This poor prediction capability for transition is primarily the result of an incomplete understanding of the physical aspects of the phenomena and the lack of suitable methods to analytically represent such complex flow phenomena.

This paper describes the results of an experimental boundary layer transition program which focuses upon one aspect of transition - the effect of nosetip bluntness on cone frustum transition.

Over 25 years ago, when early blunting studies were initiated (e.g., Brinich⁶ and Moeckel⁷), it was assumed that the frustum transition Reynolds number remained unchanged as a result of nosetip bluntness and that the movement of transition was due to a reduction of the local Reynolds number resulting from total pressure losses through the bow shock. There is no doubt that Reynolds number reduction produces a large effect which can have a major influence upon the location of boundary layer transition in hypersonic flow. Even small amounts of nosetip bluntness generates entropy layers which influence the local flow conditions for large distances downstream on the frustum. Within this region where the entropy layer is being consumed by the boundary layer the boundary layer edge conditions reflect the lower Mach numbers and lower unit Reynolds numbers of the fluid which has gone through the strong portion of the bow shock. Since the total pressure losses through a normal shock increase rapidly with increasing free stream Mach number, the Reynolds number reduction for a given configuration is strongly dependent upon free stream Mach number. Experiments by Stetson^{8,9} have shown that the maximum rearward movement of transition on a slender cone at $M_\infty = 9.3$, relative to a sharp cone, was about twice that at $M_\infty = 5.9$; this difference being in direct proportion to the differences in the Reynolds number reduction (the transition Reynolds numbers were approximately the same in both cases). Reynolds number reduction information is extremely important in the interpretation of nosetip bluntness effects on frustum transition; however, this is not the major issue since this information is readily obtainable, with uncertainties being related only to the accuracy and the limitations of the flow field program being utilized. The major problem area is associated with understanding how nosetip bluntness affects

boundary layer stability and transition on the frustum.

In retrospect it may be said that the early assumption that the local transition Reynolds number was constant along a cone with nosetip bluntness was a poor one. It was later discovered that large variations in transition Reynolds number existed between transition on the nosetip and transition on the frustum of a cone, sometimes being different by more than two orders of magnitude. For example, transition experiments on blunt bodies with highly cooled boundary layers, such as spherical configurations, have consistently found low transition Reynolds numbers; often less than 500,000 (based on surface distance) and 300 (based on momentum thickness), (e.g., Stetson¹⁰, Anderson¹¹ and Demetriades¹²). Based upon the Mach number independence principle, it would be expected that transition on such configurations would be essentially independent of free stream Mach number. However, on the frustum of a slender, blunt cone, where the entropy layer produced by the blunt nosetip has been mostly swallowed by the boundary layer, significantly larger transition Reynolds numbers have been observed, with the magnitude being Mach number dependent (e.g., Berkowitz, et al¹³, Wright and Zoby¹⁴ and Maddalon and Henderson¹⁵). Local Reynolds numbers, based on surface distance, exceeding 50×10^6 have been obtained. However, this information did not provide much guidance in regard to the possible movement of transition on the frustum with increasing free stream Reynolds number, other than to suggest the possibility of a transition jump from the frustum to the nosetip, since transition Reynolds number variations through the entropy layer swallowing region were unknown. Additional transition experiments (e.g., Stetson and Rush-ton¹⁶, Softley¹⁷, Muir and Trujillo¹⁸, and Stetson¹⁹) have subsequently indicated that nosetip bluntness makes significant changes in the local transition Reynolds number along the frustum.

It is known that many parameters influence boundary layer stability and transition. It is also known that in some situations one parameter may dominate and control transition (e.g., roughness). An interesting development resulting from these present experiments is the apparent multiplicity of parameters which have dominant roles when transition occurs within the entropy swallowing region. There may be as many as three different dominant effects, all a consequence of the nosetip, and each representative of a particular region of the entropy layer. The local transition Reynolds number had large variations throughout the entropy layer swallowing region and these variations very likely reflected a shift of dominant roles.

A characteristic feature of hypersonic flow over a sphere-cone configuration is that the high pressure gas generated by the nosetip bow shock overexpands as it travels down the frustum, requiring a recompression to arrive at the "proper" pressure at some downstream location on the frustum. Thus, an adverse pressure gradient on the frustum is a fundamental feature of hypersonic flow over sphere-cone configurations, with the magnitude and extent of the region (in terms of S/R_N) being primarily a function of free stream Mach number and cone angle.

It is known from both stability theory and experiments that adverse pressure gradients

generally produce early transition by generating a lower critical Reynolds number (the Reynolds number at which disturbances first start to amplify) and larger amplification rates of the boundary layer disturbances. However, the magnitude of the adverse pressure gradient effect on transition on sphere-cone configurations is unknown. Although a number of people have expressed concern about this problem, this author does not know of any experiments to investigate this phenomenon. This present investigation includes the results of transition experiments on an axisymmetric model designed in such a manner as to eliminate the adverse pressure gradient.

Transition experiments provide information on the location of the breakdown of laminar flow and, alone can provide only limited information regarding the fundamental questions involving the dominant instabilities and the switching of dominant instability roles. However, they can provide guidance and assistance for future stability experiments and analytical studies, which hopefully can provide more complete answers.

Finally, a word of caution is injected regarding the use of these present data. It was not the intent of this investigation to generate transition correlations to be used for design purposes, but rather to try to better understand the phenomena involved. The generality of the present data is unknown since the effects of various flow field and configuration parameters which possibly influence transition have not been determined.

2.0 Experimental Apparatus and Procedures

The experiments were conducted in the Flight Dynamics Laboratory (FDL) Mach 6 wind tunnel and the Arnold Engineering Development Center (AEDC) Tunnel F. The location of boundary layer transition was obtained from heat transfer measurements.

The FDL Mach 6 tunnel is a blow-down facility operating at a reservoir temperature of 1100°R and a reservoir pressure range of 700 to 2100 psia, corresponding to a Reynolds number per foot range of 9.7×10^6 to 30.3×10^6 . The test core of approximately 10 inches is produced by a contoured axisymmetric nozzle with a physical exit diameter of 12.3 inches. Additional details of the tunnel can be found in Reference 19. The test model for the Mach 6 tunnel was a thin-skin (nominally 0.025 inches), 8-degree half angle cone containing two rays of thermocouples. The base diameter of the model was 4 inches and the model had nosetips with the following bluntness ratios; $R_n/R_b = 0, 0.01, 0.02, 0.03, 0.04, 0.05, 0.10, 0.15, 0.20, 0.25$ and 0.30 . Nominal model surface finish was 15 microinches (rms) and the blunt nose tips were polished before each run. The model was cooled between runs so that the model surface temperature would always be the same at the start of each run (approximately 540°R). Heat transfer rates were calculated from the increase in the wall temperature of the model, during a time interval of one-half second, after the model arrived at the tunnel centerline, using standard thin-skin data reduction techniques. T_w/T_o was generally in the range of 0.52 to 0.58.

*For example, the General Electric Co. proposed to the Air Force in the mid sixties a boundary layer transition experimental program of this type. However, the program was not implemented.

A second model for the Mach 6 wind tunnel was designed without an adverse pressure gradient. Based upon inviscid flow field calculations, the radial dimensions of a cone were increased by just the amount required to keep the flow from over-expanding, thus providing an axisymmetric configuration without an adverse pressure gradient. The nosetip starts with a 0.2 inch spherical radius (the same as the 10% blunt nosetip on the sphere-cone model) which extends beyond the sonic point.

Figure 1 is a sketch of the resulting configuration and the calculated pressure distribution. It can be seen that only small changes in the cone dimensions were required to eliminate the adverse pressure gradient.

The thin-skin model was instrumented with thermocouples and surface pressure instrumentation.

The AEDC Tunnel F is an arc-driven wind tunnel of the hotshot type and capable of providing Mach numbers from about 7 to 13 over a Reynolds number per foot range from 0.2×10^6 to 50×10^6 . The test gas was nitrogen. This test was conducted with the 40-inch exit diameter contoured nozzle at a nominal free stream Mach number of 9. Because of the relatively short test time, the model wall temperature remained essentially invariant from the initial value of approximately 540°R, thus $T_w/T_o = 0.20$ to 0.38 . Since the tunnel operated with a constant volume reservoir, the reservoir conditions decayed with time. Timewise variations in Reynolds number permitted acquisition of data at different Reynolds numbers for the same run. The test model for Tunnel F was a 48-inch, 7-degree half angle cone with eight nose bluntness ratios, $R_n/R_b = 0, 0.01, 0.03, 0.05, 0.07, 0.10, 0.15,$ and 0.37 . The model contained 75 coaxial surface thermocouples and 10 surface pressure gages. Nominal model surface finish was 30 microinches (rms) and the blunt nosetips were polished before each run. Additional details of Tunnel F and the model instrumentation can be found in Reference 20.

Sharp cone transition data from the Mach 6 tunnel were compared with the correlations of Pate²¹. Pate made an extensive study of the relationship between wind tunnel freestream disturbances and boundary layer transition and developed a method to predict boundary layer transition in wind tunnels with Mach number, unit Reynolds number, and tunnel size as parameters. Figure 2 indicates Pate's predictions for the end of boundary layer transition on sharp cones in small size wind tunnels. The excellent agreement of these present transition data with the results of Pate indicated that boundary layer transition in the FDL tunnel is influenced by aerodynamic noise in a predictable manner, similar to the 17 wind tunnels considered by Pate. Furthermore, since the occurrence of transition on a wind tunnel model is the result of the combined effect of all disturbance parameters, such as tunnel free stream disturbances, model surface roughness, model vibration, flow angularity, etc.; the fact that transition Reynolds numbers were found to be the same in several wind tunnels would infer a similarity in the influence of the combined effect of disturbance parameters on boundary layer transition.

The AEDC Tunnel F was one of the tunnels considered in Pate's study and therefore has

demonstrated a similarity with other tunnels.

Figure 3 is a comparison of blunt cone transition data obtained from three facilities. All data are for an 8-degree half angle cone and the Mach numbers were nearly the same in all three facilities. Muir and Trujillo¹⁵ chose an 8-degree half angle cone and a Mach 6 wind tunnel to repeat shock tunnel experiments of Stetson and Rushton¹⁶. They stated, "the experiments were designed to provide an independent verification of the results reported earlier by Stetson and Rushton".

The data presented in Figure 3 illustrate the rearward displacement of transition in terms of entropy layer swallowing. Additional discussions of this manner of presenting blunting data and related blunting characteristics will be included later. The central message to be obtained from this figure is the good agreement of data obtained from different facilities. All three facilities produced the same blunting features and trends, indicating the results were not unique to the facility being used.

Generally it is not possible to avoid the occurrence of a small amount of solid particles in the flow of a wind tunnel. During a test a number of these particles are likely to impact a wind tunnel model and roughen the surface. Experience in the FDL Mach 6 wind tunnel with slender sphere-cone models has found that the only problem area is the nosetip, where particle impact can produce significant roughness after repeated use of a model. Model nosetips were polished before each run; however, the polishing only removed the surface material protruding from the small crater, and a cavity remained. Therefore, after repeated use of a nosetip the surface contained many small cavities. Later in this report reference will be made to a "smooth" nosetip. The quotation marks mean that the nosetip had been polished, but the surface still contained small cavities.

Another potential surface finish problem area is the joint where two pieces of a model are attached. The models utilized for this investigation had interchangeable nosetips which necessitated a junction behind each nosetip. Even though most of the nosetips were considered a good fit, there was concern as to whether or not this junction acted as a boundary layer tip.

A number of experiments with roughness on the frustum of a cone (e.g., Boudreau²² and Stainback²³) have found that large roughness, of the order of the boundary layer thickness, was required to trip the boundary layer when the free stream Mach number was hypersonic. To confirm that this same situation prevailed for these present Mach 6 experiments, several frustum roughness experiments were performed. A roughness patch (by grit blasting) was added to a 10% blunt nosetip configuration between S/R = 12.5 and 17.5 (this corresponded to the beginning of the adverse pressure gradient). Data were obtained for two roughness conditions, approximately 50 μ inches and 100 μ inches (rms). These roughness heights were small compared to the boundary layer thickness, which was typically of the order of 0.015 inches, but were considered to be representative of the maximum frustum roughness of this experiment. It was found that the roughness patches did not have any effect on boundary layer transition location.

Therefore, it was concluded that frustum roughness should not be an issue in these present experiments.

Additional details of transition comparisons and transition results obtained in the FDL Mach 6 wind tunnel can be found in Reference 9.

3.0 Results

3.1 Entropy Layer

The nosetip of a sphere-cone configuration in hypersonic flow generates high entropy fluid (usually referred to as the entropy layer) which is subsequently entrained in the boundary layer as the boundary layer grows on the frustum. The extent of the frustum boundary layer influenced by high entropy fluid and the boundary layer edge conditions at a given frustum station depend upon both geometric and flow parameters. For a slender cone in hypersonic flow, and particularly with the thinner boundary layers associated with a cold wall condition, the entropy layer extends for many nose radii downstream. Unless the nose radius is small the entropy layer is not likely to be entirely consumed by the boundary layer. For the wind tunnel models used in this Mach 6 investigation, any nosetip radius larger than 2% (0.04 in.) represented situations where the entropy layer was only partially entrained in the boundary layer by the end of the model.

In order to relate frustum transition location to nosetip bluntness effects, some reference to a quantity describing the entropy layer, rather than just a geometric dimension such as nosetip radius, would seem a better choice. To provide such a relationship Stetson and Rushton¹⁶ introduced the entropy swallowing length as a transition parameter. The swallowing distance is defined as the location on the cone frustum where the fluid which has gone through the strong portion of the bow shock has been swallowed by the boundary layer. The local Mach number and flow properties at the edge of the boundary layer at this location are nearly the same as would be obtained on the same cone with a sharp nosetip (see Figure 4). The swallowing distance is a somewhat ambiguous length since it depends upon the chosen shock shape and definition of the boundary of the entropy layer, and the choice of boundary layer assumptions. Therefore, one should not think of the swallowing length as a precise dimension.

It was not considered practical to make boundary layer calculations for all of the geometric and flow variations of the present investigation. Boundary layer calculations were made for several cases (using boundary layer codes of Hecht et al.⁵ and Adams et al.⁷) to obtain the variation of boundary layer edge Mach number and unit Reynolds number throughout the entropy layer swallowing region and to compare with calculated entropy swallowing lengths based upon the method of Rotta⁴. Rotta developed a method of obtaining certain boundary layer parameters as a function of a similarity parameter based upon swallowing distance, free stream unit Reynolds number, and nose radius [$X_{SW}/(Re_{\infty}/FT)^{1/3} (R_N)^{2/3}$]. The curves of Figure 5 are based upon Rotta's results. It was found that boundary layer edge Mach number and unit Reynolds number numerical results for a given free stream Mach number collapsed into single curves when the surface distance was normalized with

Rotta's swallowing distance. That is,

$$M_e = f(X/X_{SW})$$

$$\frac{(Re/FT)_e}{(Re/FT)_s} = \bar{f}(X/X_{SW})$$

For this paper the method of Rotta was used to calculate all of the entropy layer swallowing distances and boundary layer edge unit Reynolds numbers were obtained by assuming similar variations throughout the entropy layer swallowing regime.

Figure 6 presents calculations of local properties on a 8-degree half angle cone with a spherical nosetip radius of 0.04 inches in a $M_\infty = 5.9$ flow. These results were obtained with a boundary layer code²⁵ based upon integral solutions of the boundary layer equations. Also shown is the entropy layer swallowing length obtained for this situation by the method of Rotta. The calculated value of X_{SW} corresponds to a location on the cone where the boundary layer code indicated the local Mach number to be $0.97M_{SHARP}$. Thus, the calculated value of X_{SW} is considered to be compatible with these boundary layer code results. For a given cone half angle and free stream Mach number, the swallowing distance varies as $(Re_\infty/FT.)^{1/3}$ and $(R_n)^{4/3}$. Therefore, as the nose radius or the free-stream unit Reynolds number is increased, the swallowing distance also increases. The swallowing distance can become large compared to the length dimension of the configuration. The entire model is then engulfed with low Mach number and low unit Reynolds number flow. The region of local flow properties where the maximum rearward displacement of transition location occurred is also indicated on Figure 6. Thus, maximum displacement of transition location on the slender sphere-cone was found to be associated with essentially blunt-body flow. This point will be discussed in more detail later.

3.2 Mach Number Effects

Figure 7 shows blunting results for four different Mach numbers. The $M_\infty = 3.1$ data were obtained by Rogers²⁶ in a conventional wind tunnel; the $M_\infty = 5.5$ data are shock tunnel results of Stetson and Rushton¹⁰; the $M_\infty = 5.9$ results are wind tunnel data of Stetson^{8,9}; and the $M_\infty = 9.3$ data are arc driven Tunnel F facility data of Stetson^{8,9}. The transition lengths for the blunt cones were normalized by the transition length for the sharp cone of that facility. This provided a measure of the rearward displacement of transition on a cone when the sharp tip was replaced with a blunt tip. The abscissa is the transition distance

normalized by the swallowing distance. The right side of the figure ($X_T/X_{SW} > 1$) corresponds to situations where transition occurs at a location on the cone where the entropy layer has been swallowed and the conditions at the outer edge of the boundary layer are nearly the same as would be obtained if the cone had a sharp tip. The left side of the figure (X_T/X_{SW} small) corresponds to locations on the cone just downstream of the tip. If a different method of calculating X_{SW} were used which gave different values, the effect would be to shift the data to the right or left and not alter the basic trends. Data points shown with an arrow indicate conditions where the entire model had a laminar boundary layer. Transition would then occur at some unknown higher value.

The main point to observe from Figure 7 is the strong dependence of transition location upon free stream Mach number in the mid portion of the data. Large Mach numbers produced large rearward displacement of transition, relative to a sharp cone. Changes in blunt cone transition location relative to the sharp cone and between blunt cones with different free-stream Mach numbers can be related to the corresponding changes in local unit Reynolds number and changes in local transition Reynolds number. For these data, the sensitivity with free stream Mach number is primarily related to the sensitivity of unit Reynolds number reduction to free stream Mach number. For example, at the condition of maximum displacement, the transition Reynolds numbers were approximately the same for the $M_\infty = 5.9$ wind tunnel data and the $M_\infty = 9.3$ arc-driven tunnel data and the large difference in transition location was directly proportional to the difference in Reynolds number reduction. Note also that the maximum rearward displacement of transition occurred in situations where X_T/X_{SW} was small, indicating that the local Mach number was low and the flow field was essentially of the blunt-body type (see Figure 6). More details of the entropy layer effects will be included in the discussion of Figure 9.

3.3 Frustum Transition Movement with Increasing Reynolds Number

Figure 8 illustrates the forward movement of transition on a 7-degree half angle cone at a Mach number of about 9.1. At a free stream Reynolds number per foot of 5.4×10^6 , the cone had a completely laminar boundary layer. A small increase in free stream Reynolds number caused transition to appear near the cone mid-point at a local Reynolds number of about 550,000. Further increases in free stream Reynolds number steadily moved the transition location to the sphere-cone tangency point where the local transition Reynolds number was slightly over 300,000. This forward movement slowed as it progressed through the increasing favorable pressure gradient. These events occurred in a situation where the pressure gradient became increasingly more favorable, yet the transition Reynolds number decreased from 550,000 to nearly 300,000. Further increases in the free stream Reynolds number produced transition in the subsonic region of the tip, with a local transition Reynolds number of about 250,000. The local Reynolds numbers mentioned above were calculated by the finite difference boundary layer code developed by Adams²⁷ and co-workers. With the exception of the two largest Reynolds number conditions, all of the data of Figure 8 were obtained during a single run in Tunnel F. These variations in Reynolds

*Do not relate maximum transition location displacement with the X-scale, since it does not pertain to this nose radius; but, instead, think in terms of X/X_{SW} . For maximum displacement at $M_\infty = 5.9$, $X_T/X_{SW} = 0.04$. This was shown on this figure only to illustrate the local conditions that existed over the entire model with a larger nosetip, corresponding to maximum displacement.

number occurred during a 59 millisecond time period while the Mach number varied between 9.1 and 9.0 and the wall temperature remained essentially constant. All of the data shown were obtained along the same ray of the model. This situation, as in most boundary layer transition problems, reflects the results of several competing effects. The rapid movement of transition from the sphere-cone tangency point to the subsonic region of the tip is not a new observation. This transition pattern was first observed by Stetson and has been reported by several investigators since that time.

The analyses of Merkle²⁹, based upon linearized stability theory combined with nosetip roughness effects, provided an interesting comparison with this experimentally observed forward movement of transition. Merkle postulated two unstable regions on a sphere-cone; one associated with the tip, and the other with the cone frustum. He anticipated that transition on the frustum, due to the second unstable region, would occur at classical transition Reynolds numbers for cones in the appropriate Mach number regime. Merkle suggested that, with increasing free stream unit Reynolds number (such as a reentry vehicle descending), the transition location would move gradually forward on the frustum and would be generated by the second unstable region. During this time, the growth of disturbances on the nosetip would reach larger and larger amplitudes, but would not get sufficiently large to trigger transition. These disturbances in the boundary layer on the nosetip would grow for a time as they proceeded along the tip and then emerge from the unstable region associated with the tip and decay rapidly, thus being of no consequence in triggering frustum transition. At some critical free stream unit Reynolds number, the peak amplitude of disturbances in the unstable region on the nosetip would surpass the level at which significant non-linear interactions begin, and transition would jump discontinuously from the frustum to the subsonic region of the nosetip.

The experimentally observed rapid forward movement of transition on the cone frustum at a free stream unit Reynolds number of 5.7×10^6 and the resulting low local Reynolds number for transition at this condition does not seem to be compatible with the predictions of Merkle. It appears from these present results that the unstable region associated with the nosetip extends well beyond the tip and may influence frustum transition.

3.4 Entropy Layer Effects on Transition

Considerably more $M_\infty = 5.9$ data than shown in Figure 7 were obtained to better define the features of nosetip blunting effects on frustum transition and these new data are shown in Figure 9. At the top of this figure transition displacement data is shown, as in Figure 7. Presenting the data in terms of displacement indicates the resultant effect of nosetip bluntness; however, it does not indicate the relative contributions of Reynolds number reduction and changes in the transition Reynolds number. In order to consider these individual contributions it is necessary to utilize local flow field calculations. This requirement introduces new problems. First, the validity of

current numerical computations through the entropy layer swallowing region have not been adequately evaluated. And, secondly, the transition Reynolds numbers obtained do not account for the history of the boundary layer disturbances, which have been growing in a changing boundary layer. Thus, a transition Reynolds number obtained from an experimentally determined transition location and the calculated boundary layer edge conditions at that location does not provide general information regarding the stability characteristics of the boundary layer. In spite of these shortcomings, it was felt that informative trends could be identified by such a presentation of the experimental results. It is not the magnitude of the transition Reynolds numbers obtained that are considered to be significant, but the relative changes and trends. Also, even though the history of the disturbances is not known, this data set involves a comparison of similar histories.

For this comparison the transition Reynolds numbers for the blunt cones were normalized with the transition Reynolds numbers for a sharp cone, at corresponding free stream conditions. This type of presentation was selected because it showed the data trends and also provided a convenient method of observing the individual contributions of Reynolds number reduction and changes in transition Reynolds number. That is,

$$\frac{X_{TB}}{X_{TS}} = \frac{(Re_{xT})_B}{(Re_{xT})_S} \frac{(Re/FT)e_S}{(Re/FT)e_B}$$

Therefore, the transition displacement shown in the top portion of Figure 9 is the product of transition Reynolds number change and unit Reynolds number reduction, as shown in the bottom portion of Figure 9. The region of the adverse pressure gradient on the model is illustrated for the 10% and 25% blunt cones at a free-stream unit Reynolds number of 14.3×10^6 . The adverse pressure gradient and the swallowing distance do not have a unique relationship, since the adverse pressure gradient is an inviscid phenomena and the swallowing distance is primarily a viscous phenomena (e.g., the swallowing distance is influenced by wall temperature).

There are several general trends which are apparent. The transition Reynolds numbers had large variations along the cone frustum; in some cases being larger than a sharp cone and in other situations being very small, of the order of transition Reynolds numbers on a nosetip. Maximum transition location displacement due to nosetip blunting occurred in situations where transition Reynolds numbers were considerably less than a sharp cone; however, the Reynolds number reduction was large and was the dominant effect. As mentioned in the introduction, it is generally recognized that many parameters influence boundary layer transition; and, for a given situation, several effects may be competing for the dominant role. An observation of the trends of these transition data suggests that a multiplicity of dominant roles are associated with transition within the entropy layer swallowing region, with a dominant effect being related to a particular region of the entropy layer.

Three regions of the entropy layer have been identified and will be discussed individually.

* These results appeared in the unclassified literature in 1959 (Reference 28).

3.4.1 Region 1 ($X_T/X_{SW} \sim 1$)

When the entropy layer is nearly swallowed transition Reynolds numbers greater than those of the sharp cone are obtained.

The result is a small rearward displacement of transition relative to a sharp cone (increasing X_T/X_{TS} in Figure 8). This results from an increase in transition Reynolds number (which would increase X_T) and small amounts of Reynolds number reduction (which would increase X_T).

3.4.2 Region 2 ($X_T/X_{SW} \sim .10$)

As transition occurred at smaller values of X_T/X_{SW} a large reduction in transition Reynolds number resulted. This reduction very likely reflected a shifting of dominant roles of transition parameters. Even though the transition Reynolds number had been reduced by about a factor of three, the transition location (relative to the sharp cone) steadily moved rearward since the unit Reynolds number reduction effect was always larger than the reduction in transition Reynolds number.

Large variations of the flow parameters took place when the nosetip bluntness and the test conditions were such that transition occurred within the entropy layer designated between Regions 1 and 2. These changes could be observed by holding the test conditions constant and changing the nosetip radius or by holding the nosetip radius constant and changing the free-stream with Reynolds number. These changes resulted from the sensitivity of the flow parameters to the location within the entropy layer being considered. The 3% blunt nosetip provided a good example of changes that occurred with a single nosetip and details are given in the following table.

Re_∞/FT	X_T	X_T/X_{SW}	Re_{X_T}	M_e	$\frac{(Re/FT)_{eB}}{(Re/FT)_{eS}}$
9.8×10^6	11.0	.85	9.9×10^6	4.85	.82
11.2×10^6	10.7	.79	10.3×10^6	4.80	.77
12.6×10^6	10.3	.73	10.1×10^6	4.65	.69
15.4×10^6	9.4	.62	9.1×10^6	4.40	.56
18.2×10^6	8.6	.54	7.9×10^6	4.15	.45
21.0×10^6	8.0	.48	7.4×10^6	3.90	.39
23.8×10^6	7.6	.44	6.9×10^6	3.80	.34
25.2×10^6	7.3	.41	6.4×10^6	3.65	.31
28.0×10^6	6.9	.39	6.3×10^6	3.60	.29

*Stability experiments at $M_\infty = 8$ have demonstrated that small nosetip bluntness can completely damp disturbances of all frequencies in a local Reynolds number regime which corresponded to steady growth of disturbances on a sharp cone. In fact, the sharp cone disturbances had grown to sufficient amplitude to initiate 2nd mode wave breakdown at Reynolds numbers which corresponded approximately to the critical Reynolds number of the 3% blunt nosetip. However, once the critical Reynolds number was exceeded, amplification rates of the 2nd mode disturbances became larger than corresponding sharp cone amplification rates.

When Re_∞/FT was increased, X_T became smaller and X_{SW} became larger. Transition was then occurring at smaller values of X_T/X_{SW} . In this region of the entropy layer changes in X_T/X_{SW} result in large changes in local unit Reynolds number, with the local unit Reynolds number reducing as X_T/X_{SW} became smaller. The magnitude of the local unit Reynolds number for a particular case depended upon two factors; the free-stream unit Reynolds numbers and the location within the entropy layer which was considered. For the various test conditions of this example the magnitude of the local unit Reynolds number at the transition location changed only slightly even though the free stream unit Reynolds number was increased nearly a factor of three, since the reduction in X_T/X_{SW} lowered the local unit Reynolds number by a corresponding amount. The calculated transition Reynolds number then changed nearly in proportion to the transition location.

Based upon the fact that a minimum in the curve occurs near the end of the adverse pressure gradient and the well known results from stability theory and experiment that adverse pressure gradients promote early transition, it was easy to suspect that the dominant parameter had shifted from the stabilizing effect of the nosetip to the less stable effect of the adverse pressure gradient. However, subsequent experiments, with the model designed specifically to eliminate the adverse pressure gradient, indicated that the adverse pressure gradient had not become the dominant parameter. These results will be discussed in Section 3.6.

Increasing the nosetip radius produced transition at smaller values of X_T/X_{SW} . The boundary layer disturbances therefore had more growth within a boundary layer subjected to a favorable pressure gradient, with the gradient becoming increasingly stronger as X_T/X_{SW} became smaller. Intuitively it would be expected that transition Reynolds numbers would increase under such conditions, and the data did reflect an upward trend.

The left boundary or Region 2 corresponds to the maximum rearward displacement of transition, relative to the sharp cone. The maximum possible displacement is unknown, since the model had a completely laminar boundary layer. In this region the local Mach number was low and the Reynolds number reduction had reached its minimum value (for this $M_\infty = 5.9$ case, the local unit Reynolds number on the cone with nosetip bluntness had been decreased by more than a factor of seven over what it would be on a sharp cone). Transition Reynolds numbers were significantly less than would be obtained on a sharp cone; however, the unit Reynolds number reduction was a large effect and produced the maximum values of X_T/X_{TS} . For the free stream conditions of $Re_\infty/FT = 28 \times 10^6$

$$\frac{X_{TB}}{X_{TS}} = \frac{(Re_{X_T})_B}{(Re_{X_T})_S} \frac{(Re/FT)_{eS}}{(Re/FT)_{eB}}$$

$$> \frac{4.8 \times 10^6}{8.3 \times 10^6} \frac{37.8 \times 10^6}{5.16 \times 10^6}$$

$$> 4.2$$

It appeared that more than one effect was important for Region 2. Some unidentified effect was dominant, producing transition Reynolds numbers

less than those of a sharp cone. To a lesser degree, the favorable pressure gradient generated by the nosetip was significant.

3.4.3 Region 3 ($X_T/X_{SW} < .03$)

As X_T/X_{SW} became smaller the favorable pressure gradient became increasingly stronger, yet the transition Reynolds numbers became smaller. In some cases they were of the same order as nosetip transition Reynolds numbers. It appeared that some other effect, stronger than the effect of the favorable pressure gradient, had taken over as the dominant parameter. There were some characteristics of transition in Region 3 which were different from the other regions. First, transition location was not repeatable. In the other regions, repeat runs duplicated very closely the previous transition results. In Region 3 the transition location was unpredictable. When making several tests at the same free stream conditions, transition was found to occur anywhere on the frustum and sometimes the model would have a completely laminar boundary layer. Second, asymmetric transition patterns normally occurred at zero angle of attack. Unlike the other regions, large circumferential variations in transition location were obtained at $\alpha = 0^\circ$. Sometimes the model would be completely laminar on one side and have early transition on the other side. Third, the transition region was much longer than for the other cases and generally a fully turbulent boundary layer was never obtained. Fourth, it was observed that frustum transition was very sensitive to roughness on the nosetip. For smaller nosetip bluntness the surface condition of the nosetip (or the frustum) appeared to have no effect upon frustum transition. Polishing the 30% blunt nosetip before the run gave higher frustum transition Reynolds numbers or moved the transition location off the model. Primarily on the basis of this last observation, it was speculated that Region 3 was dominated by the nosetip instabilities. To further investigate this effect additional experiments were conducted with roughened nosetips and nosetips with higher wall temperatures. Following is a discussion of these additional experiments. All of the data shown in Figure 9 were obtained with solid nosetips. Due to the mass of the solid tip the surface temperature increase of the nosetip was small during the one-half second time used for the heat transfer data reduction. These nosetips did not contain thermocouples, so only an estimate of their temperature could be made. The fact that after the completion of several seconds of exposure to the flow, the tips were not too hot to touch indicated that the temperature rise during the early portion of the test was small. Additional data were obtained with 15% and 30% thin-skin nosetips. The thin-skin nosetip had a significantly different temperature history. During the injection of the model, the stagnation temperature typically increased from 540°R to about 935°R. Cooling or heating the tip before injection made only a small change in the surface temperature at the tunnel centerline. The frustum surface temperatures were the same with both the solid and thin-skin nosetips, typically in the neighborhood of 600°R (for a laminar boundary layer). Therefore, data were obtained for the following temperature ratios (T_w/T_0):

NOSETIP	FRUSTUM
≈ .55 (Solid)	.52 to .58
≈ .85 (Thin-skin)	.52 to .58

For the 30% blunt nosetip with the higher wall temperature the cone frustum was always laminar, even at the maximum tunnel conditions. For the 15% blunt nosetip there was no distinguishable effect of nosetip temperature upon frustum transition.

Nosetip roughness was increased by grit-blasting solid 15% and 30% nosetips. The entire spherical nose cap then contained 45-50 μ inch roughness. Upon completion of these experiments the process was repeated with a larger grit-size, producing 90-100 μ inch roughness. The addition of roughness to the 30% nosetip always produced early frustum transition for tunnel conditions corresponding to previous tests. The 45-50 μ inch roughness on the 15% nosetip had no effect on frustum transition; whereas, the 90-100 μ inch roughness produced both cases of early frustum transition and no effect, depending upon the free stream conditions.

The above results suggested that some critical value of nosetip Reynolds number, combined with nosetip roughness, determined whether or not the nosetip instabilities would produce early frustum transition. This was the same rationale that was applied to nosetip transition studies and resulted in the PANT correlation¹¹. Therefore, it was felt to be of interest to look at these present frustum transition data in terms of the PANT nosetip parameters. Figure 10 contains the results. All of the parameters are evaluated at the sonic point. The results of the PANT program and Demetriades are shown to indicate the conditions which produce transition on the nosetip. The data points shown are the nosetip conditions which correspond to the threshold of early frustum transition. Early frustum transition is defined as a deviation from the transition curve represented by the data of Region 2 of Figure 9. Region 3 represents the early transition for the 30% blunt nosetip; and although not shown on Figure 9, early transition with the 15% nosetip produced another branch of the curve, nearly parallel to the 30% nosetip data. The points in Figure 10 with an arrow indicate that the critical conditions were not obtained, and the direction of the arrow indicates the direction to the threshold condition. It was observed that the trend of the points followed the same trend as the nosetip transition data. This was confirmed by shifting the nosetip transition curve down (to 40% of nosetip transition) to obtain the dashed curve. It is seen that the dashed curve coincided with the data points and provided a good representation of the critical nosetip conditions which produced early frustum transition. Below the line is identified as "normal" frustum transition; that is, transition corresponding to data of Region 2 of Figure 9. Between the dashed curve and the nosetip transition curve, the nosetip is still laminar and early frustum transition occurs. These conditions are identified with the region where nosetip instabilities are dominating frustum transition.

Figure 11 is an example of typical transition results when transition occurs in Region 2 of Figure 9, referred to as "normal" frustum transition (15% nosetip bluntness). The heat transfer rates increase rapidly from the laminar rates and the transition location is easily determined, repeatable, and predictable (for this wind tunnel). Figure 12 is an example of early transition (30% nosetip bluntness), corresponding to Region 3 of Figure 9 and the region above the dashed line in

Figure 10 (the nosetip instability dominated region). Transition onset is not always well defined; there is typically a long transition region; transition is generally asymmetric at $\alpha=0^\circ$; and transition location is unpredictable. The data shown in Figure 8 is an example of this type of transition from another facility.

The close similarity of the model and test conditions of the Muir and Trujillo experiments with these present experiments provided for convenient data comparisons and will be used to further discuss the influence of nosetip instabilities on frustum transition. Due to these similarities, Figure 10 should be directly applicable to the Muir and Trujillo data, and help explain what otherwise might appear to be an inconsistency of the two sets of data. Consider first the Muir and Trujillo results with the 32% blunt nosetip at $Re_\infty/FT = 17 \times 10^6$. Transition was first observed at a surface distance of approximately 2.3 inches from the stagnation point ($Re_{x_T} \approx 610,000$) and in about 3.6 seconds transition had moved completely off the model, resulting in a completely laminar boundary layer ($Re_{x_T} > 3.4 \times 10^6$). The FDL experiments with a 30% blunt nosetip and similar free stream conditions, similar local flow frustum conditions, and similar frustum wall temperatures, always had a completely laminar boundary layer ($Re_{x_T} > 2.9 \times 10^6$). In fact, with a "smooth" nosetip, the free stream conditions had to be increased about 45% in order to obtain transition on the frustum. In situations where the nosetip conditions are believed to be important for frustum transition, the dimensions of the nosetip become important. The Muir and Trujillo model was longer than the FDL model; with a five inch base diameter, compared to four inches for the FDL model. Therefore, the 32% blunt nosetip (R_N/R_B) had a 0.8 inch radius, compared to 0.6 inches of the FDL model. The calculated Re_θ at the sonic point for the Muir and Trujillo model was 110. The nosetip roughness of the model was not known to this author, so it was not possible to determine the roughness parameter, $(k/\theta)(T_e/T_w)$. However, it appears likely that this condition corresponded to the edge of the nosetip instability dominated region of Figure 10. The calculated Re_θ at the sonic point for the FDL model at this free stream condition was 95, falling well below the nosetip instability region for a smooth nosetip. The addition of 45-50 μ inch roughness to the FDL model nosetip still resulted in a completely laminar boundary layer on the frustum. However, the 90-100 μ inch roughness was sufficient to obtain frustum transition at this free stream condition. For this condition the roughness parameter was estimated to be 0.85, which corresponded to the edge of the nosetip instability dominated region.

Muir and Trujillo repeated the experiment at a free stream unit Reynolds number of 23.6×10^6 . For this condition, transition was initially at approximately 2 inches from the stagnation point, about the same location as for the lower Reynolds number condition. Transition again moved rearward with time, but the movement was much slower than their previous case, and transition was still on the frustum 10 seconds later. The corresponding FDL model, with a "smooth" nosetip, was always laminar at this condition. However, if the nosetip was not polished before each run, transition sometimes occurred. The calculated Re_θ at the sonic point of the NOL model was 128, placing this condition clearly into the nosetip instability

dominated region even for a smooth nosetip. Re_θ at the sonic point of the FDL model was 111; therefore, with a "smooth" nosetip $[(k/\theta)(T_e/T_w) \sim 0.1]$ this condition was just below the nosetip instability dominated region. With 45-50 μ inch roughness on the nosetip $[(k/\theta)(T_e/T_w) = 0.46]$ early frustum transition was initiated at this free stream condition.

Therefore, on the basis of a comparison of frustum conditions, the NOL and FDL wind tunnel data do not seem compatible; whereas, with a comparison on the basis of nosetip conditions and with consideration of the criteria for nosetip instability dominated frustum transition, they are compatible.

3.5 Transition Movement with Time

An interesting characteristic of the nosetip instability dominated frustum transition was that generally the transition location was unsteady. In a number of tests, transition location vs time data were obtained and the transition location was always found to move downstream with time, varying in the amount of movement and the rapidity of movement. It appeared as though the greatest movement occurred with a choice of nosetip conditions corresponding to a location near the threshold line identifying the nosetip instability dominated region. Moving further above the threshold line produced slower transition movement and a more limited change. It was not possible to investigate this aspect of transition more fully due to the limitations of the operating conditions of the wind tunnel and the maximum nosetip size.

For one series of experiments with the 30% nosetip with 45-50 μ inch roughness, the roughness on the nosetip was polished off in front of one ray of thermocouples. Some pits in the surface remained after the polishing, but the surface was compatible to the nominal surface finish of most of the tests. The test conditions were selected such that the nosetip parameters on the rough side of the nosetip corresponded closely to the threshold line of Figure 10, and the "smooth" side of the nosetip was just below the line. The results are shown in Figure 13. The heat transfer data shown with circles are for the ray behind the polished portion of the nosetip and indicated a completely laminar boundary layer. The data shown with squares are for the ray behind the portion of the nosetip with 45-50 μ inch roughness and indicated early transition. Referring back to Figure 9, the circle data points correspond to the all laminar condition of Region 2. Transition location from the square data points corresponds to the early transition of Region 3. These results, as well as previously mentioned results, provide convincing evidence that in some situations frustum transition is very sensitive to what is happening on the nosetip.

*A number of checks on the steadiness of transition location when "normal" frustum transition occurred found no evidence of unsteadiness.

Looking further at Figure 13 it can be seen that the transition location was unsteady on the side with early transition. Before 2.5 seconds had elapsed, both sides of the model had a completely laminar boundary layer.

The movement of transition location with time is not a new observation. The NACA/Lewis Laboratory transition reversal data³⁰ are probably the most well known results and this phenomenon was later observed by Muir and Trujillo¹⁸. It was felt to be of interest to relate these past transition results to these present findings. The NACA wind tunnel experiments at $M_\infty = 3.12$ found that transition on a sphere cone-cylinder moved rearward with time. These data were correlated on the basis of frustum surface temperature. An estimate of the sonic point conditions for these experiments indicated that the nosetip conditions were very close to the nosetip instability dominated threshold line of Figure 10. This suggests the possibility that these transition data were not really a transition reversal resulting from frustum surface temperature changes, but may, in fact, have resulted from nosetip instabilities. The Muir and Trujillo experiments¹⁸ were very similar to this present program. Their tests were conducted with an 8-degree half angle cone in the NOL hypersonic wind tunnel at a free stream Mach number of 6. They observed that for the 32% blunt nosetip, transition moved rearward with time, similar to the NACA results. They also correlated their data with frustum wall temperature. It was noted that this phenomenon occurred only with the large nosetip bluntness and for the sharper configurations, which were subjected to the same environment and experienced similar increases in wall temperature, the transition location remained unchanged with time. Calculations of the sonic point conditions for the Muir and Trujillo data indicated that their reported transient transition data fell near the nosetip instability dominated region of Figure 10. As with the NACA results, it is suspected that the Muir and Trujillo data were dominated by nosetip instabilities and were not affected by frustum wall temperatures.

3.6 Adverse Pressure Gradient Effects

Boundary layer transition data were obtained with the special model designed to eliminate the adverse pressure gradient.

Figure 14 compares the measured model surface pressures with the design conditions. ($R_N = 0.2$ inches). The adverse pressure gradient was eliminated and much of the model (where transition occurred) had a zero pressure gradient.

*Heat transfer rates were normally based upon the surface temperature increase during a time interval of approximately $\frac{1}{2}$ second. However, due to the rapid changes in the heat transfer rates of these data, a time interval of approximately $\frac{1}{3}$ second was used. The time interval for each sequence of data is indicated. $t = 0$ is the time when the model arrived at the tunnel centerline.

** This comment applies only to the blunt configuration. The transition reversal results for a sharp cone are a separate consideration.

Figure 15 compares boundary layer transition Reynolds numbers with results from the sphere-cone configuration. Elimination of the adverse pressure gradient did not produce larger transition Reynolds numbers; but instead, significantly lower values were obtained. It appeared from these results that the adverse pressure gradient played only a minor role and the dominant effect was some upstream phenomena; perhaps related to the changes in the favorable pressure gradient. These findings have some similarity to previous shock tube transition results. In Reference 10 it was found that transition on a hemisphere configuration first occurred near the sonic point. The supersonic portion of the hemisphere always had a laminar boundary layer until transition occurred near the sonic point; at which time the entire supersonic region would experience transition, as if the boundary layer had been tripped. This result suggested that higher transition Reynolds numbers downstream of the sonic point might be obtained on a different configuration, such as ellipse, which had the sonic point located closer to the stagnation point. Such a configuration would have a lower Reynolds number at the sonic point than a corresponding hemisphere at the same free-stream conditions and perhaps delay the "tripping" of the supersonic boundary layer. Contrary to the above reasoning, transition occurred at a lower Reynolds number in the supersonic boundary layer of the ellipse than on the corresponding hemisphere. Both the ellipse and hemisphere had cylindrical aft-bodies. When transition occurred on the cylindrical portion of both configurations it was happening within a zero pressure gradient. It was found that the cylinder preceded by an ellipse always had a lower transition Reynolds number than the cylinder preceded by a hemisphere. It was concluded from these results that the boundary layer history in the nosetip region effects boundary layer transition for a considerable distance downstream.

At this time one can only speculate as to the dominant effect producing these check tube and wind tunnel transition results; however, it appears that the body curvature (or pressure gradient) in the nosetip region produces a major effect and not the pressure gradient on the aft-body. There are several documented cases of a strong favorable pressure gradient producing some relaminarization of a turbulent boundary layer (first reported by Sternberg⁽³¹⁾), indicating that a favorable pressure gradient can exert considerable control over the state of the boundary layer. In the process of eliminating the adverse pressure gradient, the upstream favorable pressure gradient became less than that of a sphere-cone. With the acceptance of the dominant role of the favorable pressure gradient and the ability of a strong gradient to relaminarize a boundary layer, it would seem reasonable that reduction of the gradient would work in the opposite direction and result in earlier transition.

The early frustum transition results shown in Figure 15 (the branch of the data curve parallel to Region 3 of the sphere-cone data, which show a sharp reduction in $Re_{x,T}$) suggests that the flow downstream of the sonic point is also very important in the establishment of the threshold conditions for early frustum transition. This special model had a spherical nosetip (0.2 inch radius) which extended beyond the sonic point. Therefore, the subsonic flow and the sonic point conditions for this nosetip were similar to those

for the sphere-cone configuration with 10% bluntness. The early frustum transition situation with the 10% blunt sphere-cone was never obtained for the conditions of this experiment, yet the threshold conditions for the special model was easily obtained, even with a smooth nosetip. It appears that the history of the flow downstream of the sonic point is important in regards to the early frustum transition condition. This would imply that the results of Figure 10 are restricted to a sphere-cone configuration; however, the general phenomena of early frustum transition is one which would be expected to exist for other configurations and other flow conditions. Another comment regarding Figure 10 is appropriate. The data shown in this figure are not meant to be interpreted as a general transition correlation, since the generality of these results is unknown. The intent was to use this data format to illustrate the phenomenon of nosetip instability dominated frustum transition.

4.0 Conclusions

1. A comparison of nosetip bluntness effects on frustum transition in three facilities (two wind tunnels and a shock tunnel) produced the same blunting features and trends, indicating the results were not unique to the facility being used.
2. The rearward displacement of transition on the cone frustum due to nosetip bluntness was found to be quite sensitive to free stream Mach number as well as to bluntness. At $M_\infty = 9.3$ transition was displaced rearward up to nine times the transition length for a sharp cone.
3. Frustum transition Reynolds numbers had large variations within the entropy layer swallowing region; in some cases being larger than those of a sharp cone, and in other situations being very small, of the order of transition Reynolds numbers on a nosetip.
4. Maximum transition location displacement, relative to a sharp cone, occurred in situations where the transition Reynolds numbers were considerably less than a sharp cone. The unit Reynolds number reduction was large and was the dominant effect.
5. It appeared that several nosetip blunting effects were competing for the dominant role when transition occurred in the entropy layer swallowing region, and the large changes in transition Reynolds number were believed to be associated with the shifting of dominant roles. Dominant nosetip blunting effects on frustum transition were tentatively identified with three regions of the entropy layer. (a) When transition occurred at location where the entropy layer was nearly swallowed ($X_T/X_{SW} \sim 1$), the nosetip apparently had a stabilizing effect upon the boundary layer since transition Reynolds numbers greater than those of a sharp cone were obtained. (b) Further forward in the entropy layer ($X_T/X_{SW} \sim 0.1$), it appeared that more than one effect was important. Some unidentified effect was dominant, producing transition Reynolds numbers less than those of a sharp cone. To a lesser degree, the favorable pressure gradient generated by the nosetip was significant. Some variations in the magnitude of Re_{X_T} could be related to the strength of the favorable pressure gradient. (c) In the early

portion of the entropy layer swallowing region ($X_T/X_{SW} < .03$), frustum transition was dominated by the nosetip flow and surface conditions. Low transition Reynolds numbers were obtained in spite of the existence of a favorable pressure gradient. There were several characteristics of transition in this region which were different from the other two regions.

6. The adverse pressure gradient on a sphere-cone configuration is not believed to play a dominant role in frustum transition.
7. The threshold conditions which produce early frustum transition are believed to be determined by the combination of the nosetip conditions and the favorable pressure gradient.
8. The downstream movement of frustum transition location with time was believed to be controlled by the nosetip region and not by changes in the frustum surface temperature.

5.0 References

1. Morkovin, M.V., "Critical Evaluation of Transition from Laminar to Turbulent Shear Layers with Emphasis on Hypervelocity Traveling Bodies", AFFDL-TR-68-149 (March 1969)
2. Morkovin, M.V. and Mack, L., "High Speed Boundary Layer Stability and Transition", AIAA Recorded Lecture Series, (1969)
3. Morkovin, M.V., "Instability, Transition to Turbulence and Predictability", AGARDograph No. 236 (May 1977)
4. Reshotko, E. "Boundary-Layer Stability and Transition", Annual Review of Fluid Mechanics, Vol 8, pp. 311-349 (1976)
5. Pate, S.R., "Effects of Wind Tunnel Disturbances on Boundary Layer Transition with Emphasis on Radiated Noise: A Review", AIAA Preprint No. 80-0431 (March 1980)
6. Brinich, P.F., "Effect of Leading-Edge Geometry on Boundary-Layer Transition at Mach 3.1", NACA TN 3659 (March 1956)
7. Moeckel, W.E., "Some Effects of Bluntness on Boundary Layer Transition and Heat Transfer at Supersonic Speeds", NACA Report 1312 (1957)
8. Stetson, K.F., "Effect of Bluntness and Angle of Attack on Boundary Layer Transition on Cones and Biconic Configuration", AIAA Preprint 79-0269 (Jan. 1979)
9. Stetson, K.F., "Hypersonic Boundary Layer Transition Experiments", AFWAL-TR-80-3062, (Oct. 1980)
10. Stetson, K.F., "Boundary Layer Transition on Blunt Bodies with Highly Cooled Boundary Layers", J.A.S. Vol. 27, pp. 81-91 (Feb 1960)
11. Anderson, A.D., "Interim Report, Passive Nosetip Technology (PANT) Program, Vol. X, Appendix, Boundary Layer Transition on Nosetips with Rough Surfaces", SAMSO-TR-74-86 (Jan 1975)

12. Demetriades, A., "Nosetip Transition Experimentation Program, Final Report, Vol II", SAMSO-TR-76-120 (July 1977)
13. Berkowitz, A.M., Kyriss, C.L., and Martelluci, A., "Boundary Layer Transition Flight Test Observations", AIAA Paper No. 77-125 (Jan. 1977)
14. Wright, R.L., and Zoby, E.V., "Flight Boundary Layer Transition Measurements on a Slender Cone at Mach 20", AIAA Paper No. 77-719 (June 1977)
15. Maddalon, D.V. and Henderson, A., Jr., "Boundary Layer Transition at Hypersonic Mach Numbers", AIAA Paper No. 67-130 (Jan 1967)
16. Stetson, K.F. and Rushton, G.H. "Shock Tunnel Investigation of Boundary Layer Transition at $M = 5.5$ ", AIAA Journal, Vol. 5, pp 899-906 (May 1967)
17. Softley, E.J., "Boundary Layer Transition on Hypersonic Blunt, Slender Cones", AIAA Paper No. 69-705 (June 1969)
18. Muir, J.F. and Trujillo, A.A., "Experimental Investigation of the Effects of Nose Bluntness, Free-Stream Unit Reynolds Number, and Angle of Attack on Cone Boundary Layer Transition at a Mach Number of 6", AIAA Paper No. 72-216 (Jan 1972)
19. Fiore, A.W. and Law, C.H., "Aerodynamic Calibration of the Aerospace Research Laboratories $M = 6$ High Reynolds Number Facility", ARL-TR-75-0028 (Feb 1975)
20. Test Facilities Handbook (Tenth Edition), Von Karman Gas Dynamics Facility, Vol. 3, Arnold Engineering Development Center (May 1974)
21. Pate, S.R., "Dominance of Radiated Aerodynamic Noise on Boundary Layer Transition in Supersonic-Hypersonic Wind Tunnels, Theory and Application", AEDC-TR-77-107 (March 1977)
22. Boudreau, A.H., "Artificially Induced Boundary Layer Transition on Blunt-Slender Cones at Hypersonic Speeds", Jour. of Spacecraft and Rockets, Vol. 16, pp. 245-251 (July-Aug. 1979)
23. Stainback, P.C., "Effect of Unit Reynolds Number, Nose Bluntness, Angle of Attack, and Roughness on Transition on a 5° Half-Angle Cone at Mach 8", NASA TN D-4961 (Jan. 1969)
24. Rotta, N.R., "Effects of Nose Bluntness on the Boundary Layer Characteristics of Conical Bodies at Hypersonic Speeds", NYU-AA-66-66 (Nov 1966)
25. Hecht, A.M. and Nestler, D.E., "A Three-Dimensional Boundary Layer Computer Program for Sphere-Cone Type Reentry Vehicles, Vol. 1, Engineering Analysis and Code Description", AFFDL-TR-78-67 (June 1978)
26. Rogers, R.H., "Boundary Layer Development in Supersonic Shear Flow", Boundary Layer Research Meeting of the AGARD Fluid Dynamics Panel, London, England, AGARD Report No. 269 (April 25-29, 1960)
27. Adams, J.C., Jr., Martindale, W.R., Mayne, A.W., Jr., and Marchand, E.O., "Real Gas Scale Effects on Shuttle Orbiter Laminar Boundary Layer Parameters", Journal of Spacecraft and Rockets, Vol. 14, pp. 273-279 (May 1977)
28. Stetson, K.F., "Boundary Layer Transition on Blunt Bodies with Highly Cooled Boundary Layers", IAS Report No. 59-36 (Jan 1959)
29. Merkel, C.L., "Stability and Transition in Boundary Layers on Reentry Vehicle Nosetips", AFOSR-TR-76-1107 (June 1976)
30. Diaconis, N.S., Wisniewski, R.J., and Jack, J.R., "Heat Transfer and Boundary Layer Transition on Two Blunt Bodies at Mach Number 3.12", NACA TN 4099 (Oct 1957)
31. Sternberg, J., "The Transition From a Turbulent to a Laminar Boundary Layer", Ball. Res. Lab., Report No. 906, Aberdeen Proving Grounds (May 1954)

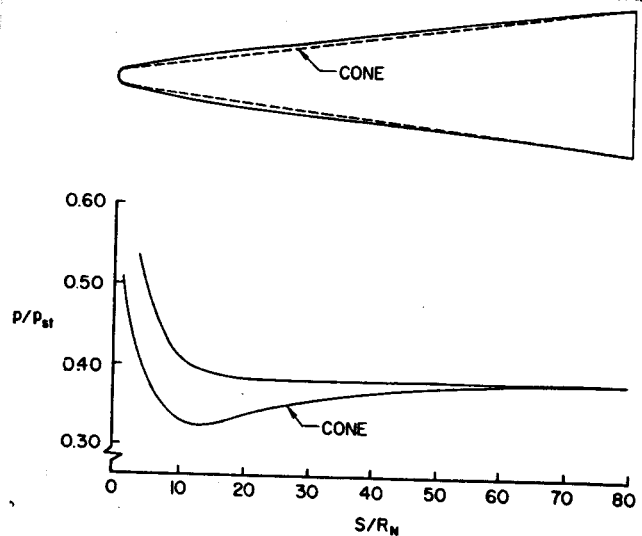


FIGURE 1 Non-adverse Pressure gradient model

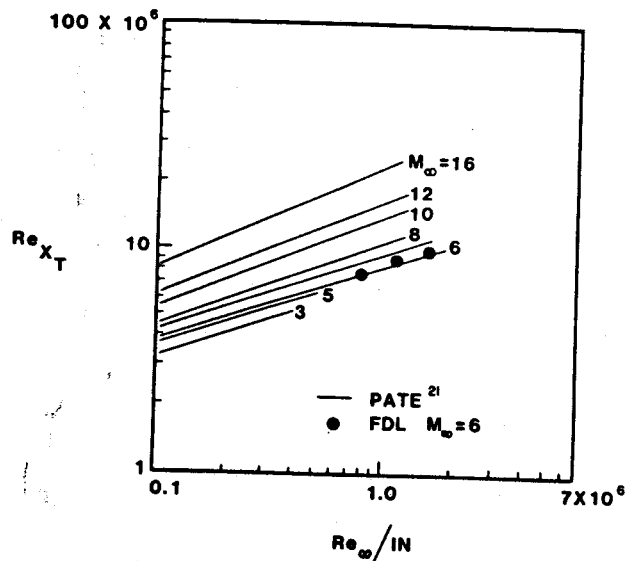


FIGURE 2 Effect of Mach number and unit Reynolds number on sharp cone transition for small size wind tunnels (Re_{X_T} is the end of transition)

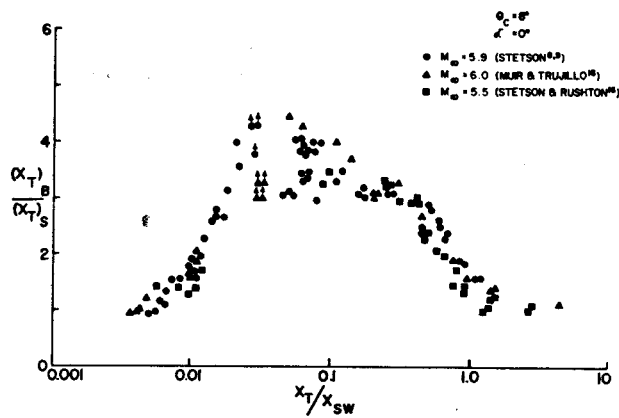


FIGURE 3 A comparison of noisetip bluntness effects on cone frustum transition in three facilities.

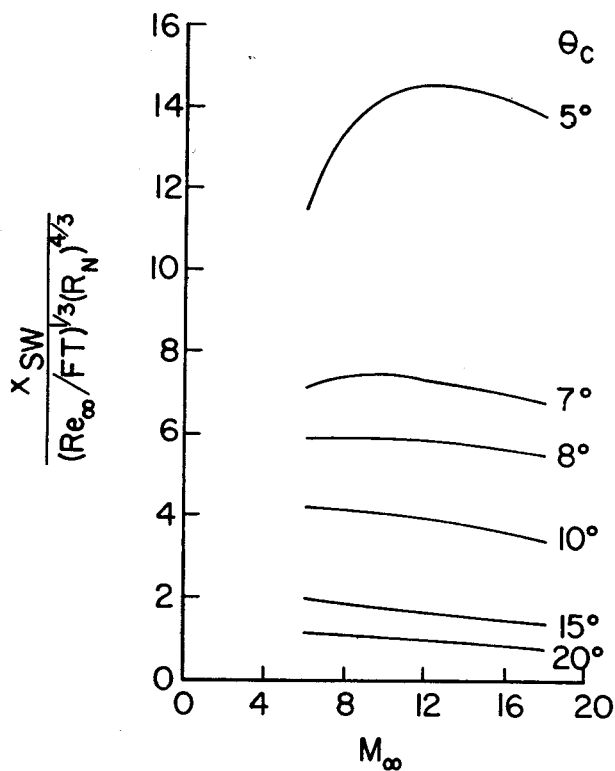


FIGURE 5 Entropy layer swallowing distance parameter.

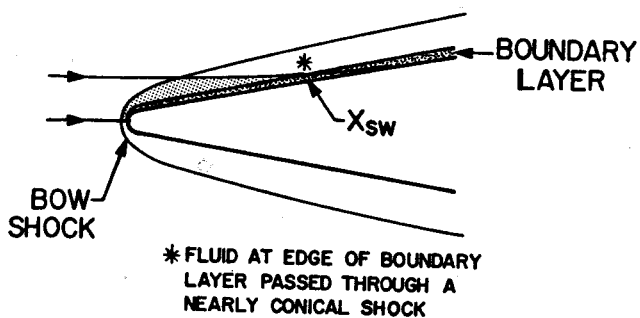


FIGURE 4 A schematic illustration of flow over a slender blunt cone

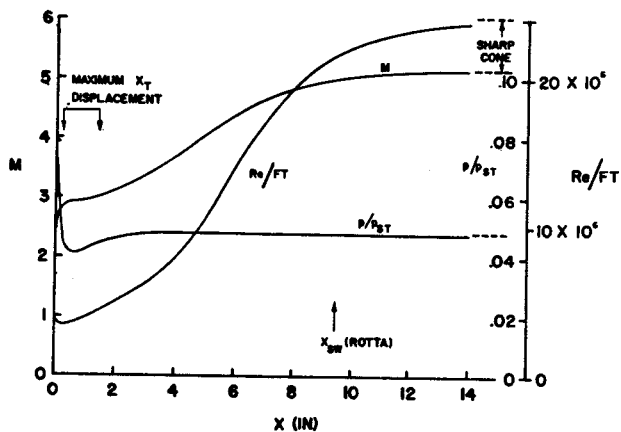


FIGURE 6 Calculations of local flow properties on a 8-degree half angle cone with 2% bluntness at $M_\infty = 5.9$.

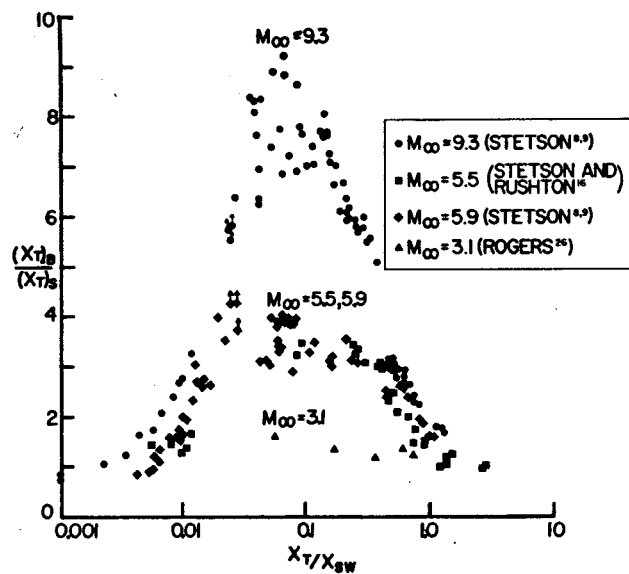


FIGURE 7 Effect of nosetip bluntness and free-stream Mach number on cone frustum transition location.

TRANSITION PROGRESSION TO NOSE TIP

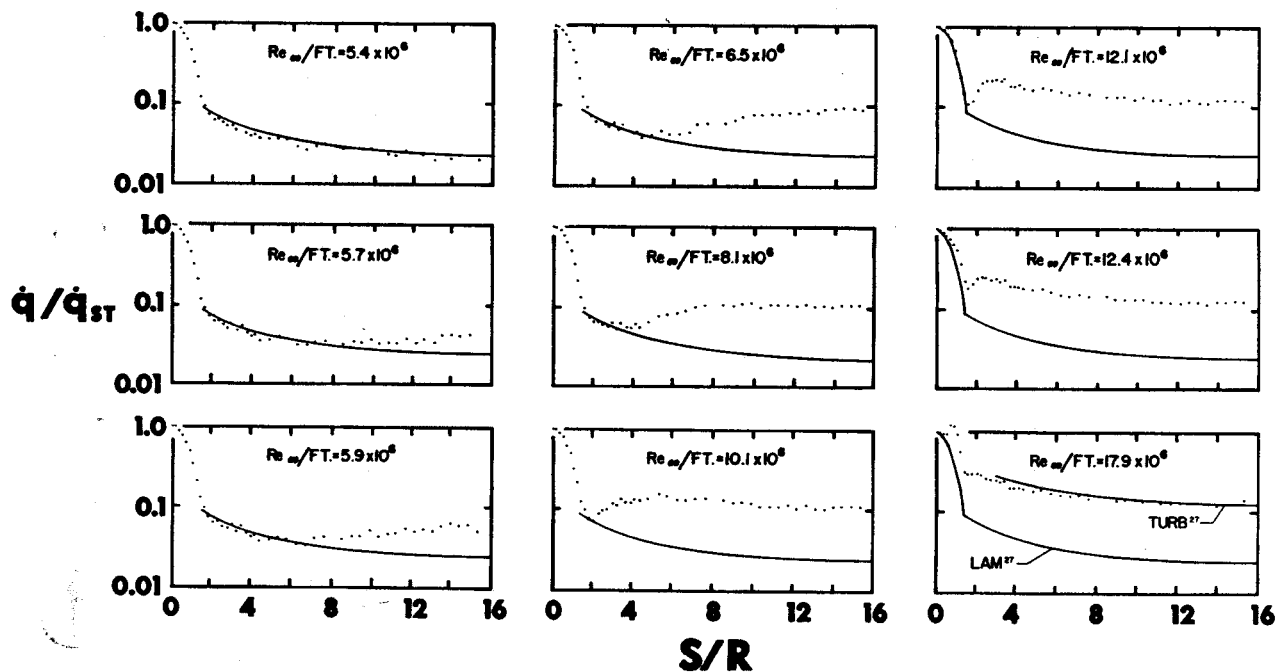


FIGURE 8 Transition movement from cone frustum to nosetip on a 7-degree half angle cone at $M_\infty = 9.1$.

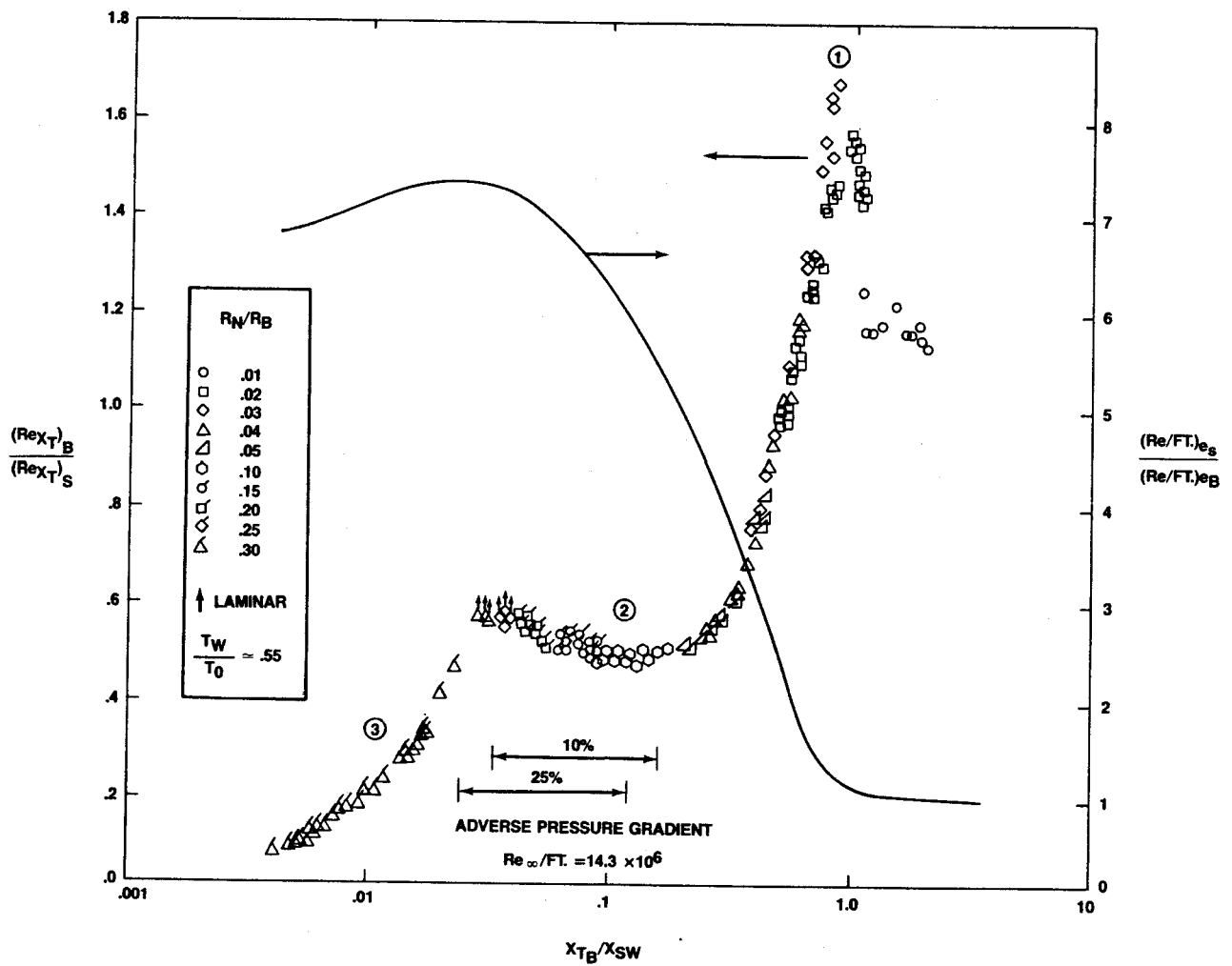
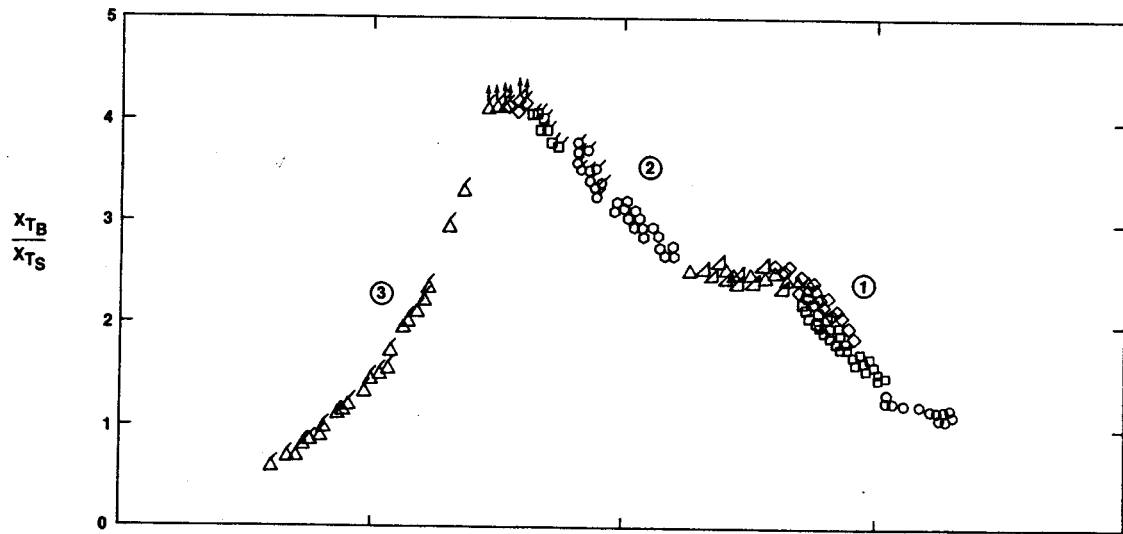


FIGURE 9 Effect of nosetip bluntness on cone frustum transition at $M_{\infty} = 5.9$.

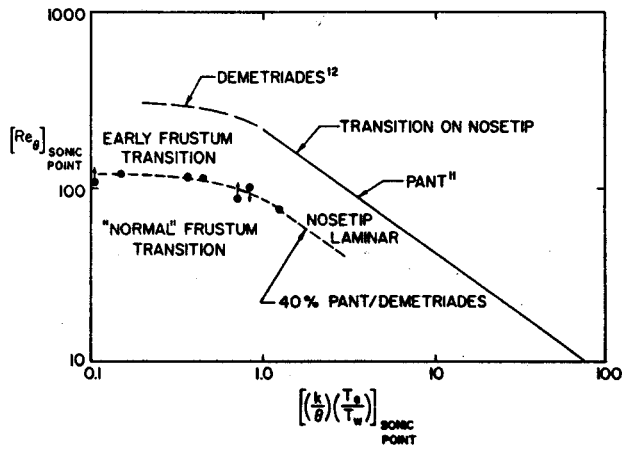


FIGURE 10 Noretip instability effects on cone frustum transition.

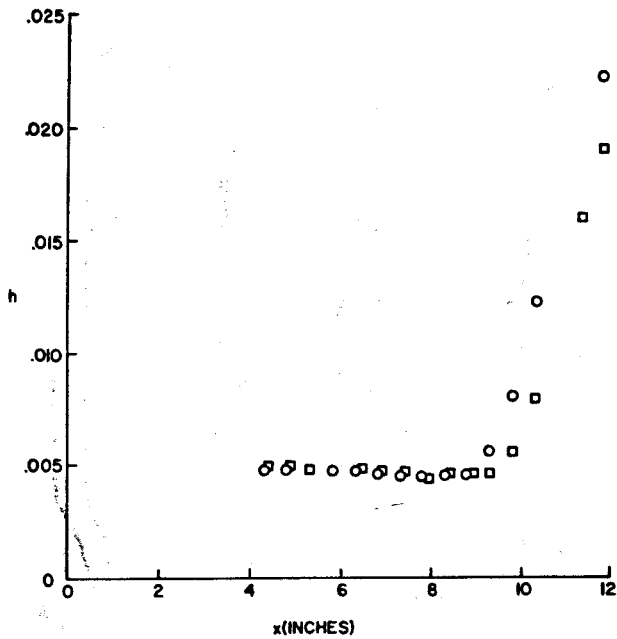


FIGURE 11 An example of "normal" cone frustum transition data

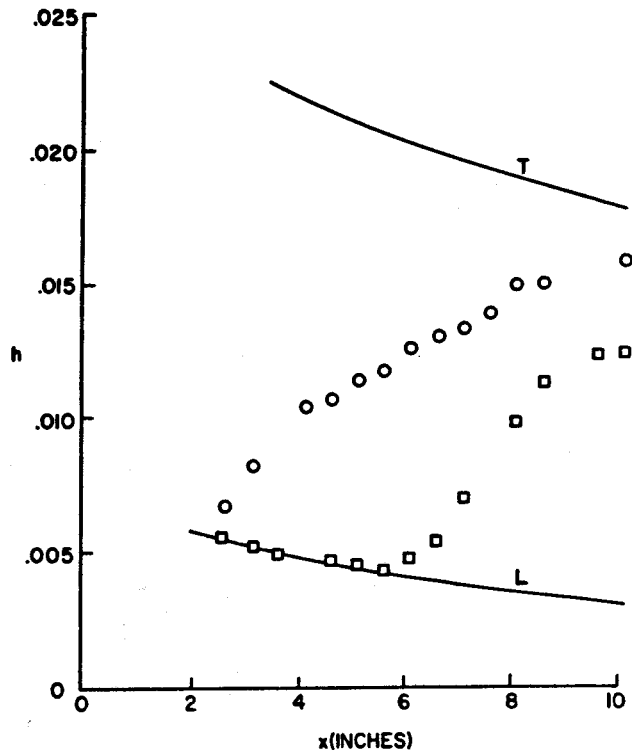


FIGURE 12 An example of noretip instability dominated frustum transition data ($\alpha = 0$)

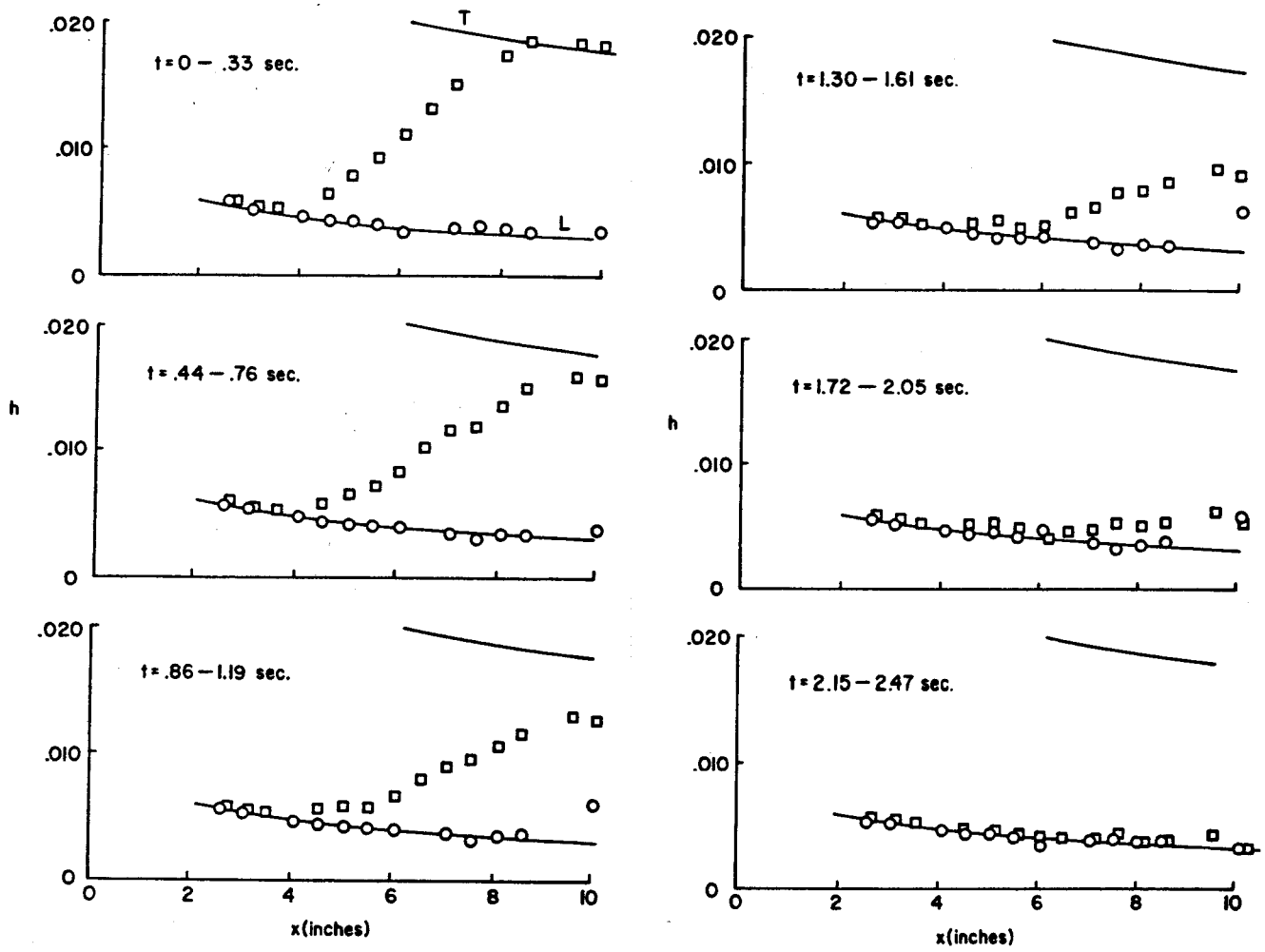


FIGURE 13 An example of unsteady transition location data.

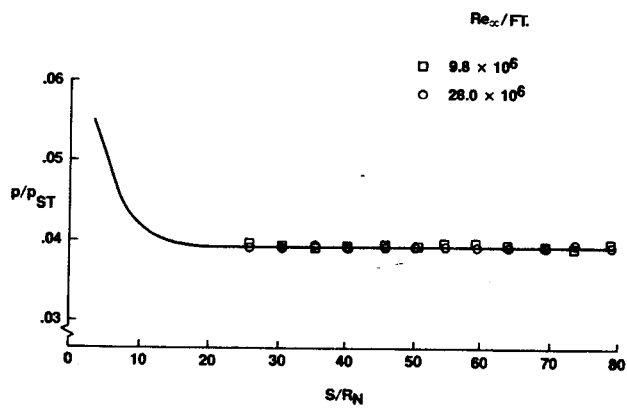


FIGURE 14 Surface pressure data for the non-adverse pressure gradient model

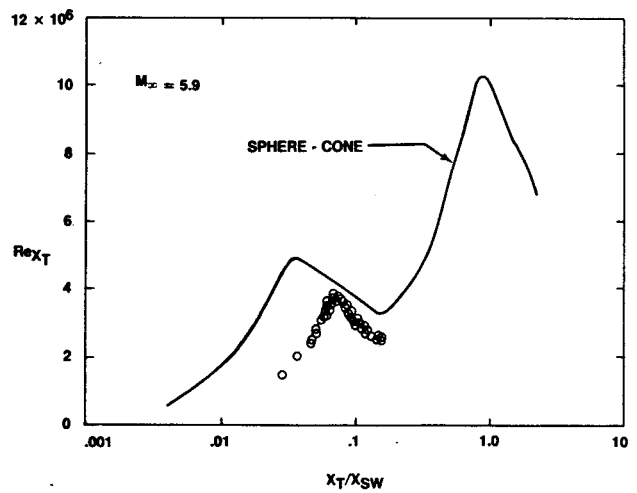


FIGURE 15 Transition Reynolds numbers for the non-adverse pressure gradient model